Interactions of 200-GeV pions in nuclei

M. Y. Lee, J. J. Lord, and R. J. Wilkes
Visual Techniques Laboratory, Department of Physics, FM-15, University of Washington, Seattle, Washington 98195
(Received 13 September 1978)

Results on multiparticle production in 200-GeV pion interactions in W and Cr are presented. Data were obtained from nuclear-emulsion plates containing embedded microgranules. The multiplicity distributions of fast charged particles have the following parameters (means and dispersions): for 53 π-W events, $\langle n_s\rangle = 14.58 \pm 1.01$, $D = 7.53 \pm 0.91$; for 57 π-Cr events, $\langle n_s\rangle = 12.53 \pm 0.64$, $D = 4.83 \pm 0.57$. Data on angular distributions and two-particle pseudorapidity correlations are presented and compared with the predictions of several current models.

I. INTRODUCTION

Collisions of hadrons with heavy nuclear targets provide valuable information on the time development of the excited hadronic state in the nucleus. Early studies of multiparticle cascades in cosmic-ray interactions and at lower accelerator energies suggested that the number of particles produced did not increase as fast with atomic mass A as expected. Fermilab experiments (such as Florian *et al.*,[1] using 200-GeV proton collisions with tungsten) gave the first evidence that the intranuclear cascade was indeed very much smaller than expected.

Results are presented from an experiment performed to study pion-nucleus interactions at high energy using nuclear-emulsion techniques. Emulsion plates (Fig. 1) containing embedded microgranules of tungsten (^{184}W) and chromium (^{52}Cr) were exposed to a 200-GeV π^- beam at Fermilab. Thus inelastic interactions in pure-element targets can be observed using emulsion as the track-detecting medium. The microgranules are small enough (diameter $\lesssim 20\ \mu$m) to ensure negligible probability of secondary interactions. The method used to prepare granule-embedded emulsion plates has been described previously.[2] Following development by conventional procedures, the plates were scanned twice, yielding 57 events in Cr and 53 in W. For each event found, we determined (1) the number of minimum-ionizing ($\beta \geq 0.7$) tracks, n_s, (2) the number of heavy tracks, N_h, and (3) the production angles of the minimum-ionizing tracks. The rescan indicated a scanning efficiency near 100% for events with $N_h > 3$ and 80% for events with $N_h \leq 3$.

We will compare our results on multiplicity and angular distributions with several theoretical models.

The energy-flux-cascade-model (EFC) proposed by Gottfried[3] considers that the essential variable of the high-energy hadron-nucleus (h-A) interaction is the energy-momentum flux of the hadronic matter (not a conventional hadron). This energy flux, after some characteristic time, behaves as a single hadron, and thus is called a "Gottfried hadron." The Gottfried hadron (with sufficient energy) will interact with $\bar{\nu}$ downstream nucleons, where $\bar{\nu}$ is estimated[4] as

$$\bar{\nu} = \frac{A\sigma_{hp}^{\text{inel}}}{\sigma_{hA}^{\text{inel}}} ; \tag{1}$$

here A is the nuclear mass and $\bar{\nu}$ is roughly the average nuclear thickness in units of mean free path of the projectile.

This model predicts an enhancement in the rapidity (y) distribution at $y < y_c$ compared to an elementary hadron-hadron (h-h or h-p) interaction where $y_c = \frac{1}{3}Y$ and Y is the incoming rapidity.

The ratio R of the average multiplicity to that of h-p interactions at the same energy is

$$R = \tfrac{2}{3} + \tfrac{1}{3}\bar{\nu} . \tag{2}$$

The EFC model has been modified by Calucci *et al.*[5] with a detailed dynamical analysis of the interaction process and has been adjusted to fit existing data. This version of the model assumes $y_c \simeq \frac{1}{2}Y$ which gives

$$R = \tfrac{1}{2} + \tfrac{1}{2}\bar{\nu} . \tag{3}$$

Figure 2(a) shows the predictions for rapidity distributions from the EFC model.

In the multiperipheral production model (MPM)[6,7] an incident particle with rapidity Y will emit a chain of particles with lower rapidities. A second chain also can be emitted well before the collision. Only particles with rapidities less than $y_c = \ln(4R/\tau_0)$ will interact with the target nucleons, where R is the nuclear radius and τ_0 is the characteristic interaction time. This gives the rapidity distribution shown in Fig. 2(b), which shows no plateau. The MPM also predicts an asymptotic form for R_y,

©1979 The American Physical Society

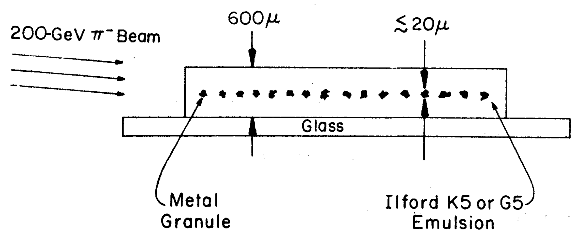

FIG. 1. Nuclear-emulsion plates with embedded metal granules.

$$R_y = \frac{\frac{1}{\sigma_{hA}^{\text{inel}}}\frac{d\sigma_{hA}}{dy}}{\frac{1}{\sigma_{hp}^{\text{inel}}}\frac{d\sigma_{hp}}{dy}} \xrightarrow[s\to\infty]{} \bar{\nu} \tag{4}$$

in the central region. A slight decrease with $A^{-1/3}$ at the high rapidity end, due to kinematic effects, is also predicted.

The predictions of a parton model by Nikolaev[8] are very similar to those of the MPM. R_y can be parameterized as $R_y = A^{\alpha}$, where α is a parameter strongly dependent on the momentum of emitted particles. In particular, in the central region $R_y = A^{1/3}$ and in the extreme forward region $R_y = A^{-1/3}$.

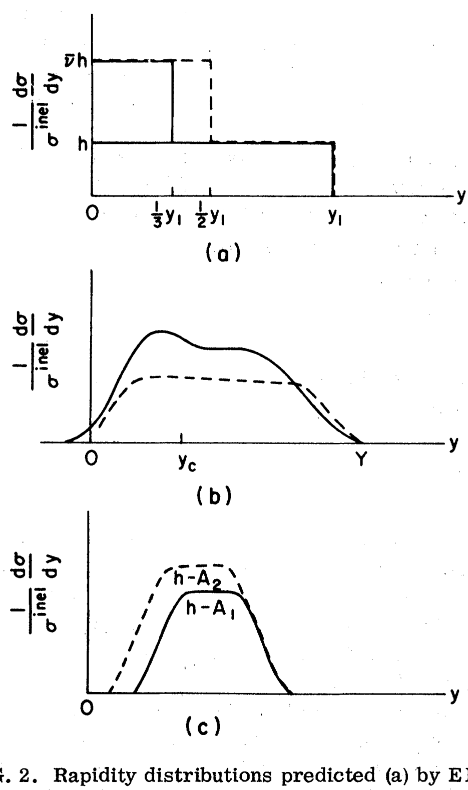

FIG. 2. Rapidity distributions predicted (a) by EFC model (solid line) and modified EFC model (dashed line) for *h-A* interactions (the *h-p* rapidity distribution is also plotted for comparison); (b) by MPM for both *h-a* (solid curve) and *h-p* (dashed curve) interactions; (c) by CTM for different size nuclei, where $A_2 > A_1$.

Another model, which also uses a parton approach, is proposed by Brodsky *et al.*[9] This model gives the multiplicity ratio R in the central rapidity region as

$$R = \frac{\bar{\nu}}{2} + \frac{\bar{\nu}}{\bar{\nu}+1} ,$$

which is also the asymptotic form of R. When the fragmentation regions are included, R is adjusted to fit data[10] at 200 GeV as follows:

$$R = \frac{\bar{\nu}}{2} + \frac{\bar{\nu}}{\bar{\nu}+1} - 0.2\left(\frac{\bar{\nu}-1}{\bar{\nu}+1}\right). \tag{5}$$

The coherent tube model (CTM)[11,12] assumes that the nucleons in a cylindrical region surrounding the incident particle path act as a single body. Therefore, the *h-A* collision can be regarded as equivalent to an *h-h* collision with the center-of-mass energy $S = A^{1/3}s = 2A^{1/3}m_p E$, where $\sqrt{s}$ is the c.m. energy of an elementary *h-h* interaction, m_p is the nucleon mass, and E is the incident energy. This model predicts that the rapidity distribution will rise in the central region and expand toward the target fragmentation region as A increases [Fig. 2(c)]. It also predicts that the scaled multiplicity distribution of *h-A* interactions will be equivalent to that of *h-p* interactions. In addition, the average multiplicities are related as

$$\langle n_s(E)\rangle_{hA} = \langle n_s(A^{1/3}E)\rangle_{hp} . \tag{6}$$

II. RESULTS

A. Fast-particle multiplicity distributions

The distribution of n_s is plotted separately for tungsten and chromium events in Fig. 3. Results are similar to those found in proton-induced interactions.[2] The n_s distribution for tungsten events has greater dispersion than that of chromium, with the average multiplicity $\langle n_s\rangle$ and the dispersion ($D^2 = \langle n_s^2\rangle - \langle n_s\rangle^2$) of the distributions being $\langle n_s\rangle = 14.58 \pm 1.01$, $D = 7.35$ for 53 π-W events, and $\langle n_s\rangle = 12.53 \pm 0.64$, $D = 4.83$ for 57 π-Cr events. The dispersions are larger than $(\langle n_s\rangle)^{1/2}$. Thus, for both sets of events, minimum-ionizing particle multiplicities are distributed more broadly than expected for a Poisson distribution.

The Koba-Nielsen-Olesen (KNO) scaling function $\psi(z)$, the multiplicitly distribution on the scaled variable $z = n_s/\langle n_s\rangle$, is a universal function independent of incident energies E for *h-h* interactions. Figure 4 shows the scaled multiplicity distribution of the tungsten and chromium events from this experiment, also showing the data from π-*p* interactions at 205 GeV from a bubble-chamber experiment,[13] the data from pion-emulsion (π-Em) interactions at 16 GeV,[14] and the data from π-Ne colli-

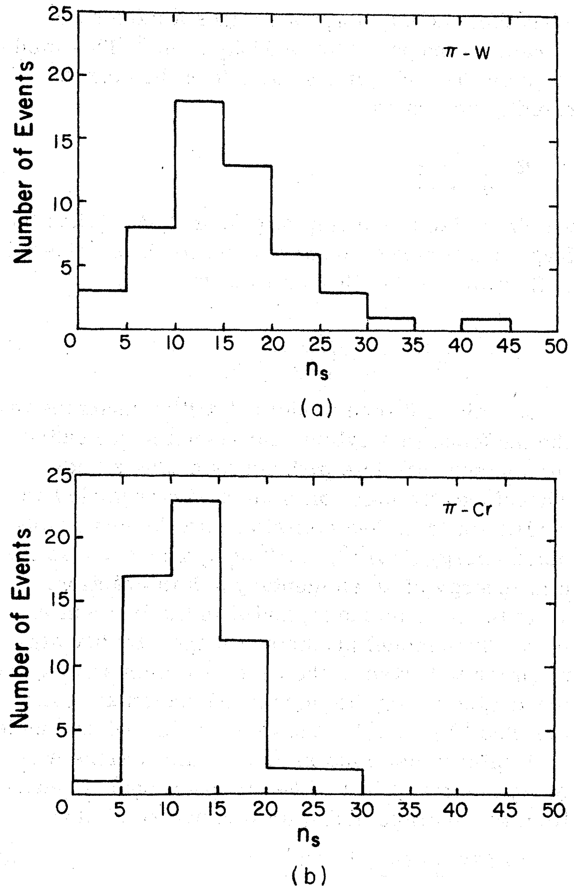

FIG. 3. Histograms of multiplicity distributions for (a) π-W and (b) π-Cr interactions at 200 GeV.

sions at 10.5 and 200 GeV.[15] All the data have been normalized to make the area beneath the curve equal to 1. The solid curve shown is the least-squares fit of a function, similar to that used

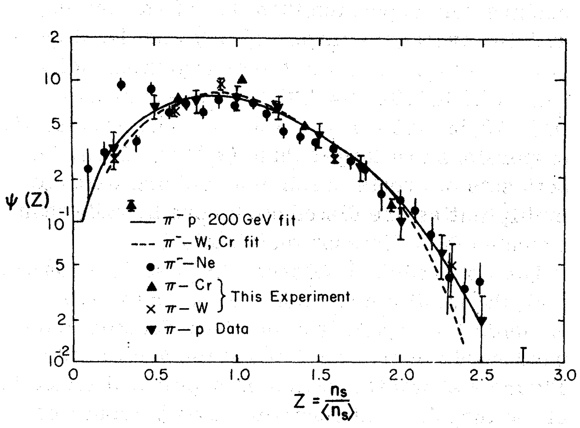

FIG. 4. Scaled multiplicity distributions, where $Z = n_s/\langle n_s \rangle$ and $\psi(Z) = \langle n_s \rangle P_n$. The solid line is the least-squares fit to Eq. (7) for π-p data, and the dashed line is for the W and Cr data from this experiment.

by Slattery,[16] to π-p data,

$$\psi(Z) = (AZ + BZ^3 + CZ^5 + DZ^7)\exp(-EZ)\,, \qquad (7)$$

while the dashed curve is for both tungsten and chromium data. The coefficients and χ^2 of both functions are summarized in Table I. The two curves are very close together for the region in which we have good statistics, in agreement with the predictions of the CTM and MPM.[7] From the observations, the scaled multiplicity distribution seems to be invariant over the energy range considered, and for different targets, within 10–15%.

For the KNO scaling hypothesis to be valid, the moments of the multiplicity distribution should be independent of energy, and the ratio of D to $\langle n_s \rangle$ is expected to be constant with increasing $\langle n_s \rangle$. This behavior is observed for proton-induced interactions.[17] In experiments using pions, measurements for nucleon and nuclear targets have been compiled by Busza[4] and Wróblewsky[17] for the energy range 50–205 GeV. These values, along with our data (corrected for scanning efficiency; see Table II), are shown in Fig. 5. Since the value of D is very sensitive to possible scanning bias against events with low multiplicity, missing events with low multiplicity tend to reduce the value of D. Thus the experimental results represent lower limits for this quantity. To correct the data for events with $N_h \leq 3$, an overall scanning efficiency[18] of 80% is assumed for both chromium and tungsten events.

The solid line is a linear least-squares fit over all the data points (see Fig. 5), yielding $D = (0.551 \pm 0.015)\langle n_s \rangle - (0.437 \pm 0.121)$ with $\chi^2/\mathrm{DF} = 1.03$, which gives a significantly smaller slope than that of the proton data.

B. R vs $\bar{\nu}$

The dependence of the ratio R on $\bar{\nu}$, where R is defined[19] as

$$R = \frac{\langle n_s \rangle_{\pi A}}{\langle n_{ch} \rangle}\,, \qquad (8)$$

and $\langle n_{ch} \rangle$ is the number of charged relativistic particles produced in π-p collisions, is important for differentiating predictions made by different models. The value of $\langle n_{ch} \rangle$ in π-p interactions at 200 GeV is taken from the bubble-chamber value[13]: $\langle n_{ch} \rangle = 8.02 \pm 0.12$.

In order to calculate the average number of collisions $\bar{\nu}$ in nuclei using Eq. (1), we use 200-GeV π-p cross sections,[13,20–22] $\sigma_t \simeq 24.2$ mb and $\sigma_{inel} = 21.2$ mb. The inelastic cross section for hadron-nucleus collisions (σ_{hA}) has been measured[22] at Serpukhov in the 6–60 GeV/c momentum range. It was found that, very much as in hadron-hadron

TABLE I. Coefficients from the least-squares fits of the function for scaled multiplicity distribution (after Slattery, Ref. 16) $\psi(Z) = (AZ + BZ^3 + CZ^5 + DZ^7)\exp(-EZ)$ for π-nucleus and π-p interactions at 200 GeV.

	A	B	C	D	E	χ^2/DF
p-p (Ref. 16)	3.79	33.7	−6.64	0.332	3.04	
π-p	1.915	12.36	−3.105	0.194	2.705	0.026/11
π-W, π-Cr	0.052	23.21	−5.837	0.332	3.025	0.21/9

interactions, the inelastic cross sections for pion, kaon, and proton-nucleus interactions are independent of energy for $p \gtrsim 20$ GeV/c; also the inelastic cross sections for π^+ and π^- are equal within the measurement errors. The dependence of σ_{hA} on the mass number of the target A for pion projectiles can be well described by

$$\sigma_{\pi A} = (28.5)A^{0.75}\ \text{mb}\ .$$

Thus $\bar{\nu}$ is related to A as

$$\bar{\nu} = 0.744A^{0.25}\ .$$

Figure 6 shows the data from this experiment and the data from proton-nucleus and proton-emulsion[2] interactions at 300 and 200 GeV, respectively. It is found that

$$R = 1.82 \pm 0.15 \text{ for } \pi\text{-W}$$
$$= 1.56 \pm 0.10 \text{ for } \pi\text{-Cr}$$

in this experiment. Predictions of R vs $\bar{\nu}$ from different models (EFC and the asymptotic form of R in the model proposed in Ref. 9), and a best-fit curve (B) for π- and p-nucleus interactions from counter experiments of Busza *et al.*[4,10] are also shown in Fig. 6 for comparison. It is clear that most of the data points seem to agree with the prediction $R = \frac{1}{2} + \frac{1}{2}\bar{\nu}$ of most of the current models, including the modified EFC, MPM, etc., while the data of Busza *et al.* also seem to support this observation within the limit of experimental error.

A corrected value of R using an estimation of the number of nonrelativistic particles in the h-p data[10] can be expressed by

$$R^* = \frac{\langle n_s \rangle_{\pi A}}{\langle n_{ch} \rangle - 0.5}\ . \tag{9}$$

This brings the value of the ratio higher:

$$R^* = 1.94 \pm 0.16 \text{ for } \pi\text{-W}$$
$$= 1.67 \pm 0.10 \text{ for } \pi\text{-Cr}$$

and moves the data points up above the line $R = \frac{1}{2} + \frac{1}{2}\bar{\nu}$.

Note that R is not very sensitive to scanning bias. From Table II one can see that the deviations of the corrected $\langle n_s \rangle$ values from raw values are only ~4% for both π-Cr and π-W events.

C. Heavy tracks

The number of heavy tracks (N_h) emerging from the hadron-nucleus collision is believed to be a convenient measure of the degree of excitation or the effective size of the target nucleus in the interaction. The heavy tracks are mainly recoil protons (which give gray tracks, the number of which is approximately linearly dependent on the number of black tracks) and target fragments (black tracks) evaporated from the excited nucleus. It has been found that the heavy tracks are isotropically emitted in the c.m. system and are independent of the incident energy.[23] N_h depends only on the target, and probably the type of projectile.

Figure 7 gives the N_h distributions for π-W and π-Cr events. As in p-emulsion interactions at 200 GeV,[1] both the π-W and π-Cr data decrease monotonically as N_h increases. However, there are differences when compared with the results from p-Cr and p-W interactions at 300 GeV,[2] which show peaks at larger N_h values.

The average N_h values[24] from this experiment are

$$\langle N_h \rangle = 11.15 \pm 1.57$$

for π-W, and

$$\langle N_h \rangle = 8.49 \pm 0.91$$

for π-Cr. These show little difference from the 300-GeV proton results (summarized in Table III).

Table IV summarizes the coefficients of the straight lines (see Fig. 8)

TABLE II. Multiplicity data corrected for scanning efficiency.

Interaction	n_s experiment	n_s corrected	D_{exp}	D_{corr}	Number of events
π-W	14.58 ± 1.01	14.05 ± 1.00	$7.35^{+0.91}_{-0.56}$	7.50	53
π-Cr	12.53 ± 0.64	12.00 ± 0.68	$4.83^{+0.57}_{-0.35}$	5.24	57

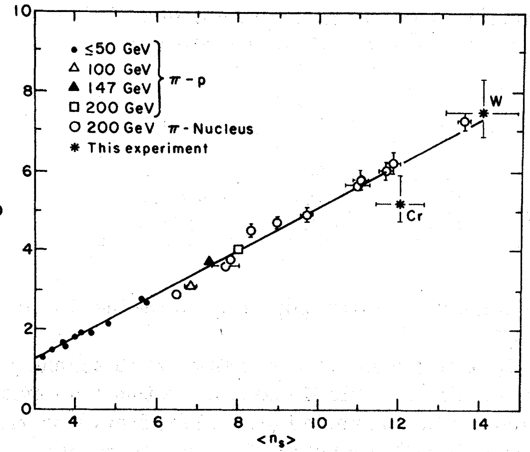

FIG. 5. Data and least-squares fit of data for D vs $\langle n_s \rangle$ where

$$D = [(\langle n_s^2 \rangle - \langle n_s \rangle^2)]^{1/2}.$$

π-W and π-Cr data from this experiment are indicated. Other points are π-p and π-nucleus data at several energies compiled by Busza (Ref. 4) and Wróblewski (Ref. 17).

$$\langle n_s \rangle = a + bN_h \tag{10}$$

which best fit the data of π- and p-induced interactions for W and Cr events at 200 and 300 GeV.

As can be seen in Fig. 8, the emulsion and W data both fit straight lines well, while the Cr data deviate at large N_h. This effect cannot be due to scanning bias, since our scanning efficiency is near 100% for large N_h. Since heavy tracks are primarily recoil nucleons and target fragments, one might intuitively expect a relatively small nucleus such as Cr ($Z = 24$) to exhibit saturation effects at $N_h \sim Z$. The N_h distribution for Cr cuts off rather abruptly at $N_h = 25-30$.

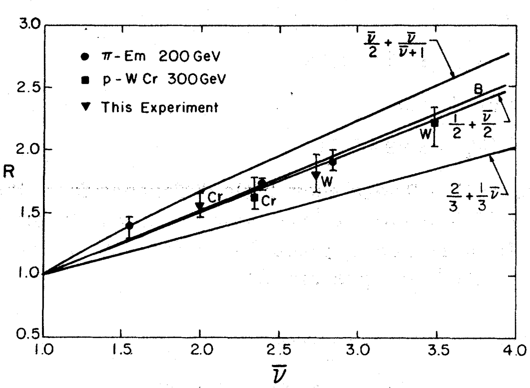

FIG. 6. R vs $\bar{\nu}$: data are shown as indicated. The lines labeled with functions of $\bar{\nu}$ are predictions from various models, while the line B is the best fit to data from a counter experiment (Ref. 10).

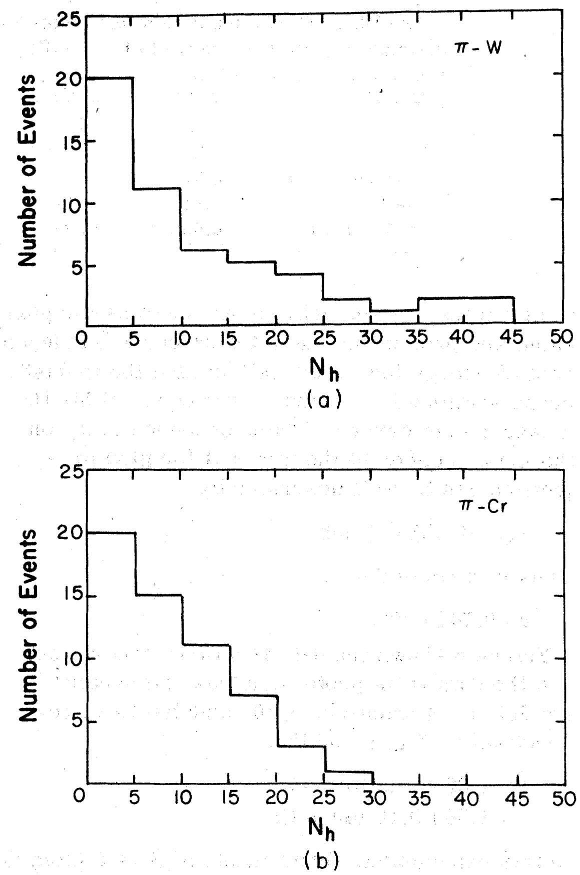

FIG. 7. Histograms of N_h distributions for (a) π-W and (b) π-Cr interactions at 200 GeV.

D. Angular distribution

The inclusive distributions for fast particles are presented in terms of the pseudorapidity variable $\eta = -\ln\tan(\theta/2)$, where θ is the laboratory production angle of the relativistic particle. This quantity is easily derived from the experimental measurements and also represents the high-energy limit of the true rapidity,

$$y = \tfrac{1}{2}\ln\frac{E+P_l}{E-P_l} \xrightarrow[s\to\infty]{} -\ln\tan\frac{\theta}{2},$$

where P_l is the longitudinal momentum. It is found[4] that the y and η distributions differ only slightly in the low rapidity region (within one rapidity unit).

The distributions shown in Fig. 9 have been normalized to correspond to a single interaction. Error bars have been plotted for some bins to give an idea of the range over which distributions may fluctuate. A cutoff was made at $\eta = 7.0$, due to limitations of angular measurement accuracy. This corresponds to an angular resolution of 2

TABLE III. $\langle N_h \rangle$ for hadron-nucleus interactions.

Projectile	Target (A)	Number of events	$\langle N_h \rangle$	Incident energy	$\bar{\nu}$
p	W(184)	51	12.9 ±1.2	300 GeV	3.49
p	Cr (52)	39	7.2 ±0.07	300 GeV	2.36
π	W(184)	53	11.15±1.57	200 GeV	2.74
π	Cr (52)	57	8.49±0.91	200 GeV	2.00

mrad. Thus, measurements of pseudorapidity for particles with $\eta \gtrsim 7$ are not significant; these were therefore combined with the particles within the bin 6.5–7.0.

In Fig. 9, both the average pseudorapidities $\langle\eta\rangle$ and the c.m. rapidity $\eta_{\text{c.m.}}$ for π-W and π-Cr interactions, also indicated with arrows, are found to be

$$\langle\eta\rangle = 2.954 \pm 0.053 \text{ for } \pi\text{-W} ,$$

$$\langle\eta\rangle = 3.131 \pm 0.057 \text{ for } \pi\text{-Cr} ,$$

$$\eta_{\text{c.m.}} = \ln\frac{\sqrt{s}}{m_p} = 3.03 ,$$

where m_p = mass of the nucleon.

Figure 10 shows the variation in the η distribution of hadronic interactions with target size (or target mass A). Shown in Fig. 10 are the η distributions from this experiment, along with those from π-emulsion interactions[25] and π-p interactions[26] at 200 GeV. One can see that η distributions seem to be independent of the size of the target in the projectile fragmentation region. An increase in the target fragmentation regions as A is increased is also seen. The existence of a depletion in the extreme forward region, predicted by the MPM and Nikolaev and observed in some experiments,[27,28] is not apparent within the statistical accuracy allowed by this experiment. The EFC model predicts that there exists a critical value η_c where $\eta_c \approx y_c$ and is independent of A, and that only in the region $\eta \leq \eta_c$ do the η distributions deviate from one another, with the nature of the deviation independent of the targets. However, in this experiment, it is hard to find a clear η_c value from the data in Fig. 10. Also, the location of the peak in the η distribution shifts toward lower rapidities as A increases. These features seem not to agree with what is expected from the EFC model. Observations similar to those discussed above are also given in Ref. 29. In the target-fragmentation region, the rapidity distribution rises with increasing A, but the expansion toward the direction of low rapidity (predicted by the CTM and also seen in the data of Ref. 10) is not observed. Similar behavior is observed in the p-nucleus[2] and π-Em data,[25] which used N_h as a means of estimating the A of the nucleus involved in a collision. Differences between our data and that of Busza *et al.* may be due to the substantial corrections needed for the counter data at large angles. One advantage of the emulsion technique is its 4π acceptance.

From the above observations on the pseudorapidity distribution, our data would seem to agree most closely with the predictions of the MPM. Further, the growth of the height of the η distributions with A in the central region, which is ~85% for π-W and ~45% for π-Cr with respect to π-p data, is much faster than predicted by the CTM. We find that R_y [defined in (4)] fits the form $R_y \sim A^{\alpha}$ with $\alpha \simeq 0.2$ in the central region, while both the MPM and the Nikolaev models predict $R_y = A^{1/3}$ in the central region at asymptotic energies. Our statistics are too low for a meaningful fit in the fragmentation regions.

The η distributions are also plotted for events binned according to N_h. Figures 11 and 12 are for π-W and π-Cr interactions, respectively. As the target nucleus becomes more strongly excited, as evidenced by increasing N_h, the centroids of the η distributions shift to smaller values. This implies that N_h is a relevant quantity for measuring the influence of the target nucleus on multiparticle

TABLE IV. Coefficients from linear least-squares fit of data to $\langle n_s \rangle = a + bN_h$.

Interaction	E (GeV)	a	b	χ^2/DF	From
π-Em	200	8.24±0.28	0.51 ±0.02	0.02	Ref. 32
π-W	200	9.98±1.11	0.414±0.044	0.04	This experiment
π-Cr	200	11.36±1.92	0.13 ±0.14	0.12	This experiment
p-Em	300	9.2 ±0.5	0.72 ±0.04		Ref. 2
p-W	300	11.0 ±2.4	0.57 ±0.15	0.01	Ref. 2

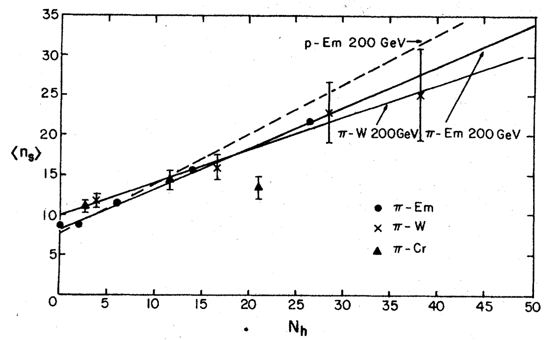

FIG. 8. $\langle n_s \rangle$ vs N_h data for π-W, π-Cr, and π emulsion at 200 GeV as indicated. Best-fit curves for π emulsion, π-W and p-emulsion interaction data are included for comparison.

production.

It should also be noted that in both π-Cr and π-W interactions, a bimodal structure not seen at lower N_h may exist in the η distributions for $N_h \geq 11$. This has been pointed out by Anzon *et al.*,[29] whose data show the first maximum located at $\eta = 3-4$ and the second maximum growing with increasing N_h and shifted toward low rapidities. Since it is not seen in experiments using protons or other projectiles the bimodality is believed to be a property peculiar to pion-nucleus interactions at high energies.

E. Two-particle pseudorapidity correlations

Two-particle pseudorapidity correlations have been extensively studied as a tool for understanding multiparticle production. Experiments on correlations in p-p interactions have been done both at Fermilab and at CERN ISR. In addition, recent investigations have been made in this area using nuclear emulsion (i.e., with mixed nuclei) as the target.[30,31] In this experiment, we obtained data

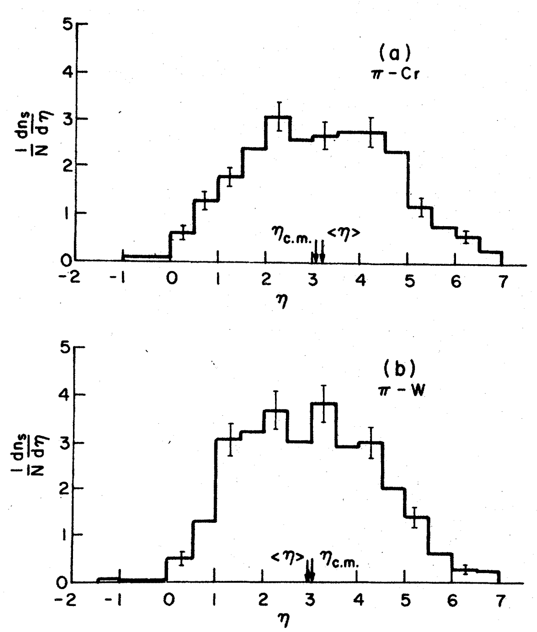

FIG. 9. Pseudorapidity distribution, normalized to one event, for (a) π-Cr and (b) π-W interactions at 200 GeV.

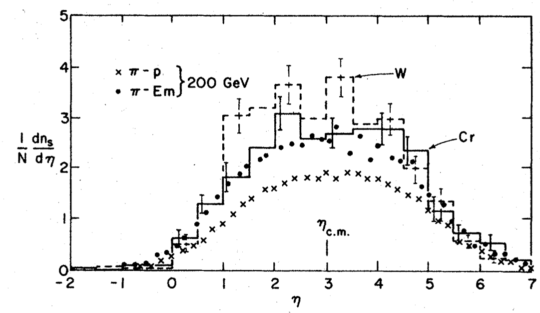

FIG. 10. Comparison of pseudorapidity distributions at 200 GeV for different target sizes: π-p and π-emulsion data are as indicated; the solid histogram is for π-Cr interactions, the dashed histogram is for π-W.

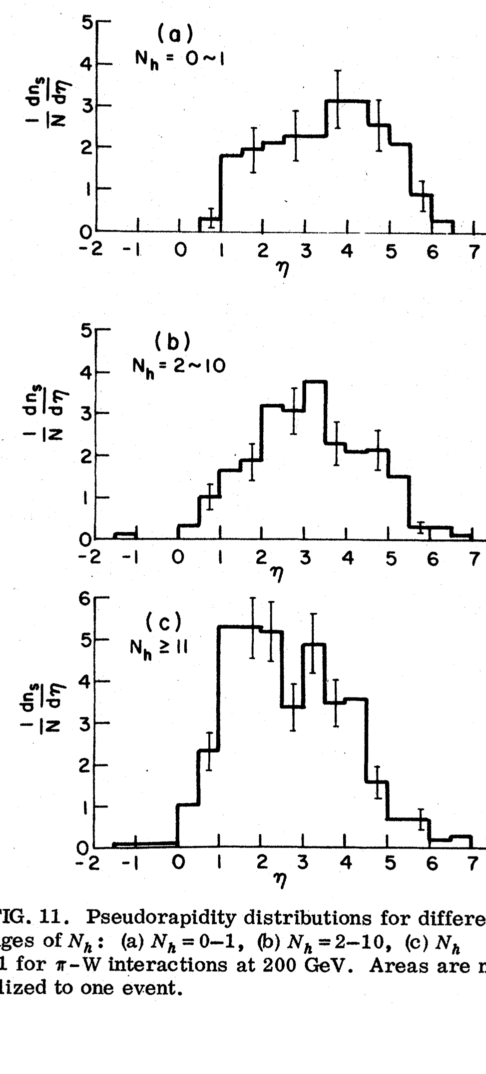

FIG. 11. Pseudorapidity distributions for different ranges of N_h: (a) $N_h = 0-1$, (b) $N_h = 2-10$, (c) $N_h \geq 11$ for π-W interactions at 200 GeV. Areas are normalized to one event.

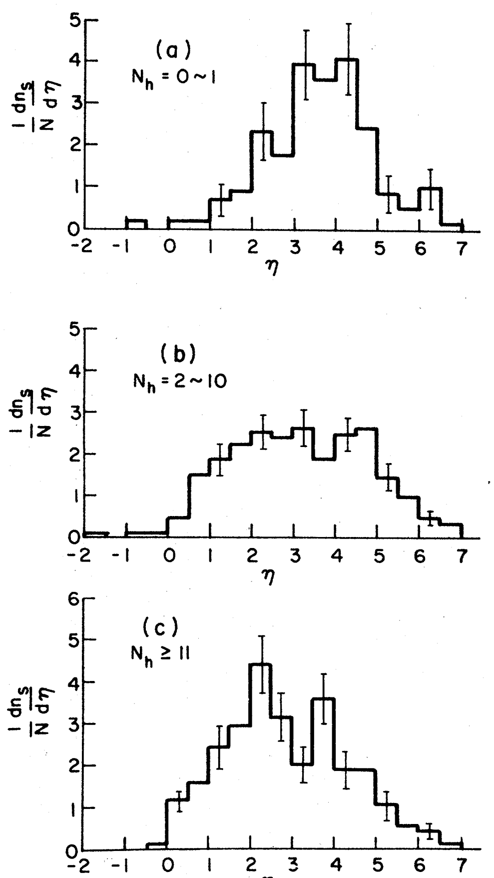

FIG. 12. Pseudorapidity distributions for different ranges of N_h: (a) $N_h = 0-1$, (b) $N_h = 2-10$, (c) $N_h \geq 11$, for π-Cr interactions at 200 GeV. Areas are normalized to one event.

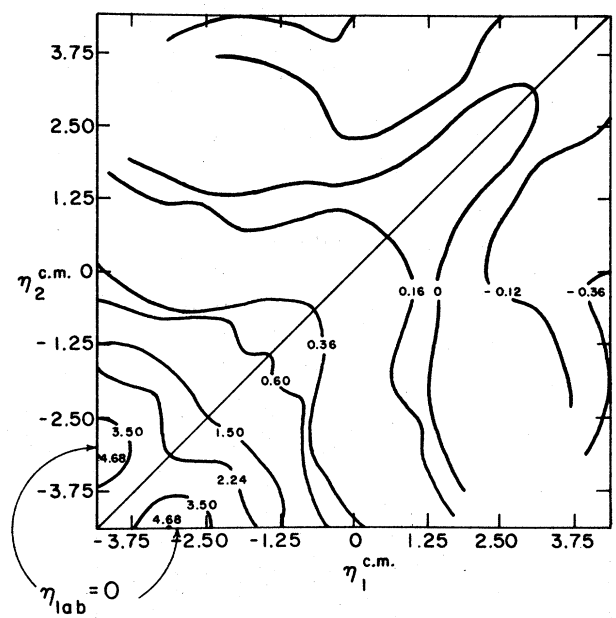

FIG. 13. Two-dimensional contour plot of the correlation function $\mathcal{R}(\eta_1, \eta_2)$ for π-W interactions at 200 GeV in the c.m. system.

on the correlation behavior for hadronic interactions with pure element targets. However, few theoretical models have made predictions about these features. The CTM considers that the nucleus acts as a whole in the h-A interaction: Thus, the two-particle rapidity correlations would be expected to be similar for h-p and h-A interactions. Other models discussed in Sec. I make no explicit predictions regarding correlations. The two-particle correlation function is defined as

$$\mathcal{R}(\eta_1, \eta_2) = \frac{\sigma^{\text{inel}} \dfrac{d^2\sigma}{d\eta_1 d\eta_2}}{\dfrac{d\sigma}{d\eta_1}\dfrac{d\sigma}{d\eta_2}} - 1$$

$$= \frac{N_T N_2(\eta_1, \eta_2)}{N_1(\eta_1) N_2(\eta_2)} - 1 , \qquad (11)$$

where

σ^{inel} = total inelastic cross section,

N_T = total number of events,

$N_1(\eta_1)$ = total number of particles at pseudorapidity η_1,

$N_2(\eta_1, \eta_2)$ = total number of particle pairs with pseudorapidity η_1 and η_2 in the same event.

Figures 13 and 14 show the general features of

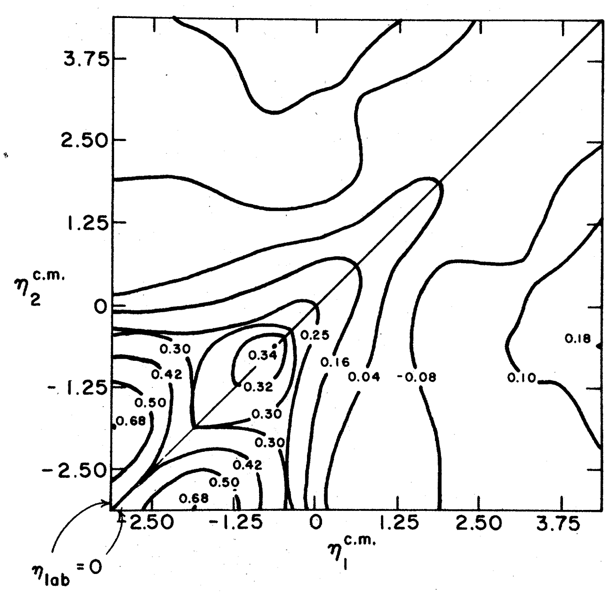

FIG. 14. Two-dimensional contour plot of the correlation function $\mathcal{R}(\eta_1, \eta_2)$ for π-Cr interactions at 200 GeV in the c.m. system.

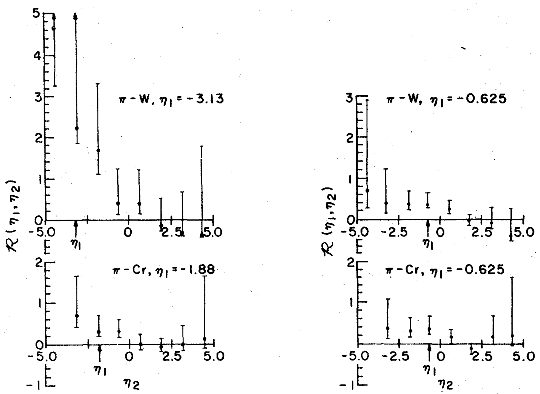

FIG. 15. Correlation function $\mathcal{R}(\eta_1, \eta_2)$ at several different fixed η_1 for π-W and π-Cr interactions at 200 GeV in the c.m. system.

the two-particle correlation for π-W and π-Cr interactions respectively with a contour plot of the function $\mathcal{R}(\eta_1, \eta_2)$ on the η_1, η_2 plane in the c.m. system. Only the area where we have reasonable statistical confidence in $\mathcal{R}$ is plotted. The contours of constant $\mathcal{R}(\eta_1, \eta_2)$ are obtained by linear interpolation. Zero pseudorapidities in the lab system are indicated by arrows. Figure 15 shows slices of the contour plots at fixed η_1.

The contour plot of $\mathcal{R}$ for π-nucleus interactions is very different from that derived from proton targets. The plot is no longer symmetric about the line $\eta_1 = -\eta_2$, nor is the maximum at the center of the graph. (The remaining symmetry about the line $\eta_1 = \eta_2$ is due to the definition of $\mathcal{R}$.) Instead, there are strong correlation centers in the low rapidity region, due to the influence of the target nucleus. Also, in the c.m. system, there are very weak correlations (or none at all) between the forward-cone and the backward-cone particles. Particles in the very forward cone of the projectile region are uncorrelated, while backward particles show substantial $\mathcal{R}$ values. These facts imply that the mechanism involved in producing forward particles is different from that involved in producing backward particles, which are believed (e.g., in the MPM) to be produced in a much more complicated multistep process. The mechanisms described in Refs. 6 and 8 would tend to produce the correlations observed.

The fact that correlations are very different in h-h and h-A interactions contradicts the CTM prediction, and tends to support the interaction mechanism described in Refs. 6 and 8.

III. CONCLUSIONS

Despite low statistics, several significant conclusions can be drawn from this experiment.

The multiplicity distribution for π-nucleus interactions displays KNO scaling behavior similar to that seen for p-p interactions. $\langle n_s \rangle$ increases linearly with the number of heavy tracks N_h, except for the unusual case of π-Cr interaction at large N_h. The multiplicity ratio R depends on $\bar{\nu}$, the average number of collisions in the target nucleus, in a relationship $R = \frac{1}{2} + \frac{1}{2}\bar{\nu}$, which is consistent with most of the current models in the present energy range. To see if this feature agrees with the MPM or the parton model of Ref. 8, one would need to see if R approaches an asymptotic value at very high energy.

The inclusive pseudorapidity distributions for π-nucleus interactions are almost independent of target mass A in the forward cone, while in the target fragmentation region the η distribution rises as A increases. This behavior contradicts the EFC model but not the MPM. If one groups events by the degree of target excitation using N_h as a parameter, one can see that the η distribution shifts in the direction of low rapidity as N_h increases, while for large N_h the η distribution develops an apparent second maximum and shows a bimodal structure.

A strong but almost constant correlation is found for particles with rapidities in the target fragmentation regions. Particles in the forward cone are very weakly (or not at all) correlated with those in the backward cone. No correlation is found among particles in the projectile fragmentation region. These facts suggest substantially different production mechanisms for the two regions.

ACKNOWLEDGMENTS

We wish to thank Dr. J. R. Florian and Dr. J. W. Martin for useful discussions, Dr. Lou Voyvodic and the Fermilab staff for assistance with the emulsion exposure, and H. Tepfer for invaluable technical assistance. This work was supported by the U.S. Department of Energy, under Contract No. EY765062225/TA27.

We are indebted to the late Professor J. H. Weis, whose patient explanations were invaluable in aiding our understanding of current theoretical work.

[1]J. R. Florian *et al.*, in *Experiments on High Energy Particle Collisions—1973*, proceedings of the International Conference on New Results from Experiments on High Energy Particle Collisions, Vanderbilt University, edited by Robert S. Panvini (AIP, New York, 1973), p. 126.
[2]J. R. Florian *et al.*, Phys. Rev. D 13, 558 (1976).
[3]K. Gottfried, Phys. Rev. Lett. 32, 957 (1974).
[4]W. Busza, in *High Energy Physics and Nuclear Structure—1975*, proceedings of the Sixth International Conference, Santa Fe and Los Alamos, edited by D. E. Nagle *et al.* (AIP, New York, 1975), p. 211.
[5]G. Calucci, R. Jengo, and A. Pignotti, Phys. Rev. D 10, 1468 (1974).
[6]J. H. Weis, Acta Phys. Polonica B7, 851 (1976).
[7]A. Capella and A. Krzywicki, Phys. Lett. B67, 84 (1977).
[8]N. N. Nikolaev, review paper given at International Seminar on Particle-Nucleus Interaction, Miramere-Trieste, 1976 (unpublished).
[9]S. J. Brodsky, J. F. Gunion, and J. H. Kühn, Phys. Rev. Lett. 39, 1120 (1977).
[10]W. Busza, paper submitted to the XVIII International Conference on High Energy Physics (unpublished); lectures given at the VII International Colloquium on Multiparticle Reactions, Tutzing, 1976 (unpublished).
[11]Y. Afek *et al.*, Technion–Israel Inst. of Tech Report No. Technion-PH-76-48, 1976 (unpublished).
[12]G. Berlad, A. Dar, and G. Eilam, Phys. Rev. D 13, 161 (1976).
[13]D. Bogert *et al.*, Phys. Rev. Lett. 31, 1271 (1973).
[14]A. J. Buras *et al.*, Phys. Lett. 47B, 251 (1973).
[15]J. R. Elliott *et al.*, Phys. Rev. Lett. 34, 607 (1973).
[16]P. Slattery, Phys. Rev. D 7, 2073 (1973).
[17]A. Wróblewski, Acta Phys. Polonica B4, 857 (1973).
[18]C. J. Waddington, Suppl. Nuovo Cimento 19, 37 (1961).
[19]B. Andersson and I. Otterlund, Nucl. Phys. B88, 350 (1975). Note that some authors define R differently, e.g., Eq. (9).
[20]E. L. Berger *et al.*, Nucl. Phys. B77, 365 (1974).
[21]D. Fond *et al.*, Phys. Lett. 53B, 290 (1974).
[22]S. P. Denisov *et al.*, Nucl. Phys. B61, 62 (1973).
[23]Alma-Ata-Leningrad-Moscow-Tashkent Collaboration, Yad. Fiz. 19, 1046 (1974) [Sov. J. Nucl. Phys. 19, 536 (1974)].
[24]No correction has been made for heavy tracks stopped in the granules. Correction factors calculated for wire targets [B. Jakobsson and E. Stenlund, Nucl. Instrum. Methods 153, 1 (1978)] are of the order of 5–10%, and corrections for granules will be considerably smaller.
[25]B. Furmanska *et al.*, Kraków Inst. of Nucl. Phys. report, 1977 (unpublished).
[26]N. N. Biswas (private communication) (University of Notre Dame, Notre Dame, Indiana).
[27]D. Chaney *et al.*, Phys. Rev. Lett. 40, 71 (1978).
[28]L. S. Osborne *et al.*, Phys. Rev. Lett. 40, 1624 (1978).
[29]Z. V. Anzon *et al.*, Nucl. Phys. B129, 205 (1977).
[30]G. Baroni *et al.*, Nucl. Phys. B103, 213 (1976).
[31]B. Wosiek, Acta Phys. Polonica, B8, 493 (1977).
[32]W. Wolter, Kraków (private communication).